JOURNAL OF VIROLOGY, Aug. 1987, p. 2395–2406
0022-538X/87/082395-12$02.00/0

Vol. 61, No. 8

Novel Transcription Map for the B19 (Human) Pathogenic Parvovirus

KEIYA OZAWA,* JAMSHED AYUB, HAO YU-SHU, GARY KURTZMAN, TAKASHI SHIMADA, AND NEAL YOUNG

Cell Biology Section, Clinical Hematology Branch, National Heart, Lung, and Blood Institute, Bethesda, Maryland 20892

Received 14 January 1987/Accepted 20 April 1987

The B19 parvovirus, a small single-stranded DNA virus of 5.4 kilobases, is pathogenic in humans. B19 has remarkable specificity for erythroid progenitor cells and has been propagated in vitro only with human erythroid bone marrow. Replication of viral DNA and the viral protein products of B19 appear similar to those of other animal parvoviruses. However, B19 transcription had unusual features in comparison with that in other animal parvoviruses. At least nine overlapping poly(A)$^+$ transcripts were identified in infected cells; all but one contained large introns. B19 differed from other parvoviruses in (i) the initiation of all transcripts at a strong left side promoter (p_6) and the absence of a functional internal promoter; (ii) the presence of short 5′ leader sequences of about 60 bases and very large introns for RNAs encoded by the right side of the genome; (iii) two separate transcription termination sites, in contrast to cotermination at the far right side of the genome for other parvoviruses; (iv) the probable utilization by three transcripts of a variant polyadenylation signal (ATTAAA or AATAAC) in the middle of the genome; and (v) the abundance of two unique transcripts from the middle of the genome which did not code for capsid proteins. The unusual transcription map of B19 suggests that regulation of the relative abundance of transcripts occurs by splicing and termination-polyadenylation events rather than by promoter strength. In combination with the published nucleotide sequence, the novel transcription map separated the pathogenic B19 virus at a molecular level from other animal parvoviruses and human adeno-associated virus.

The B19 human parvovirus was discovered serendipitously in the sera of normal blood bank donors in 1975 (12) and was subsequently identified in seroepidemiologic studies (2) and experimental human infection (1) as the causative agent of fifth disease (erythema infectiosum), a common childhood exanthem and a polyarthralgia syndrome in adults (30, 40); transient aplastic crisis in patients with underlying hemolysis (11, 28); and some cases of spontaneous abortion (7, 19). More recently, chronic B19 infection has been strongly implicated in severe bone marrow depression in an immunosuppressed child (G. Kurtzman, K. Ozawa, B. Cohen, G. Hanson, R. Oseas, and N. S. Young, N. Engl. J. Med., in press).

In transient aplastic crisis, abrupt cessation of erythropoiesis leads to sudden severe anemia. The tropism of B19 parvovirus for erythroid progenitor cells has been demonstrated in vitro (25, 43). B19 virus is a potent inhibitor of erythroid colony formation and is directly cytotoxic to a cell at about the late erythroid progenitor cell (CFU-E) stage (42). Propagation of the virus has been accomplished only in primary cultures of human bone marrow cells (26). In these suspension cultures, B19 replication correlates with the erythroid cell content at the time of inoculation and with the presence of erythropoietin, and replication fails to occur in wholly myeloid pathologic bone marrow or within the leukocyte fraction of normal bone marrow.

Parvoviruses are the smallest DNA-containing viruses to infect animal cells (35). Their seeming simplicity has made them attractive to molecular biologists. Parvoviruses have a very limited genome of about 5 kilobases (kb) of single-stranded DNA. One genus, the dependoviruses, requires helper functions provided by coinfection of adenoviruses or herpesviruses for productive infection; human adeno-associated viruses are dependoviruses. The autonomous parvoviruses, which replicate in the absence of other viruses, are common animal pathogens; feline panleucopenia virus, Aleutian mink disease virus, minute virus of mice, and Kilham rat virus are examples of members of this genus. Despite differences in their biological behavior, both types of parvovirus have similar genetic organizations. The coding potential of the short genome is increased by utilization of overlapping transcripts and multiple reading frames. Structurally, their DNA is characterized by the presence of terminal hairpin structures that serve as initiation sites for replication through double-stranded intermediate forms. Two or three structurally similar capsid proteins are encoded by the right side of the genome by separate but overlapping RNA species. One to three noncapsid proteins that are thought to provide replicative functions are encoded by the left side. In the parvoviruses studied so far, separate promoters drive transcription from the left side and the middle of the genome.

The pathogenic B19 human virus is, for a member of the *Parvoviridae* family, remarkable in its highly restricted tissue range. The molecular basis of this unusual biologic behavior remains uncertain. In erythroid bone marrow cells cultured in vitro, the pattern of B19 DNA replication resembles that of other parvoviruses (26). The protein species that compose the capsid and the noncapsid proteins also are analogous in number and size to those of other parvoviruses (13, 27). As we report here, however, the B19 transcription map differs in several fundamental aspects from that of other *Parvoviridae*.

MATERIALS AND METHODS

Cell culture. B19 parvovirus was propagated in human erythroid bone marrow cells that were obtained from patients with sickle cell disease after informed consent and

* Corresponding author.

were cultured in suspension (26). Serum containing parvovirus (Minor II; 60 μg of B19 DNA per ml) was incubated with the low-density mononuclear cell fraction for 2 h at 4°C to allow adsorption and cultured in the Iscove modification of Dulbecco medium–20% fetal calf serum–0.5 U of recombinant erythropoietin (Amgen Biologicals, Thousand Oaks, Calif.) per ml for 2 days at 37°C, in 5% CO_2, and at 95% humidity. HeLa cells were cultured under similar conditions in the Iscove modification of Dulbecco medium–10% fetal calf serum.

In situ hybridization. B19-infected bone marrow cells were separated into erythroid and leukocyte fractions by a panning technique with anti-leukocyte monoclonal antibodies as described previously (K. Ozawa, G. Kurtzman, and N. Young, Blood, in press); cytocentrifuge preparations of the erythroid fraction were fixed in 4% *para*-formaldehyde in phosphate-buffered saline and stored in 70% ethanol at 4°C until use. In situ hybridization was performed as described previously (Ozawa et al., Blood, in press) by the method of Harper et al. (17), except for the use of a ^{35}S-labeled-nick-translated pYT103 DNA probe (a full-length B19 clone) (33). Because samples were not denatured, hybridization with RNA and single-stranded DNA was discriminated by prior treatment of cell preparations with RNase A (100 μg/ml for 3 h at 37°C) or S1 nuclease (500 U/ml for 30 min at 37°C).

RNA analysis. RNA was prepared from control and infected bone marrow cells by guanidinium hydrochloride extraction. Poly(A)$^+$ RNA was selected on messenger-affinity paper (Amersham Corp., Arlington Heights, Ill.) (39). Northern analysis was performed by 1.5% formaldehyde gel electrophoresis, transfer to a nylon paper (Gene Screen Plus; New England Nuclear, Corp., Boston, Mass.), and hybridization with ^{32}P-labeled pYT103 (22). For Northern analysis, samples were further treated with RNase-free DNase I (Promega Biotec, Madison, Wis.) in the presence of ribonuclease inhibitor (RNasin [1 U/μl]; Promega). Restriction enzyme-digested fragments of pYT103 were used as molecular weight markers (undigested, 5.11 kb; *Pst*I digested, 3.14, 1.25, and 0.72 kb; *Bam*HI-*Kpn*I digested, 3.9, 1.03, and 0.18 kb). One-dimensional neutral and alkaline analyses and two-dimensional S1 nuclease analysis were performed by the methods described by Berk and Sharp (5) and Favaloro et al. (15), respectively. For S1 nuclease analysis, the pYT103 insert that was isolated by *Eco*RI digestion was used as a probe. RNA samples from cells and the pYT103 DNA probe were dissolved in 30 μl of hybridization buffer (40 mM PIPES [piperazine-*N*,*N*′-bis(2-ethanesulfonic acid; pH 6.4], 1 mM EDTA, 400 mM NaCl, 80% formamide). After heating at 85°C for 15 min, samples were hybridized for 3 h at 52°C and digested with S1 nuclease (Bethesda Research Laboratories, Gaithersburg, Md.) in 300 μl of reaction buffer (280 mM NaCl, 30 mM sodium acetate [pH 4.4], 4.5 mM zinc acetate, 20 μg of denatured calf thymus DNA per ml, 200 U of S1 nuclease per ml) for 30 min at 15°C for neutral and two-dimensional gels and at 37°C for alkaline gels. After agarose gel electrophoresis and Southern transfer, protected fragments were detected by hybridization with nick-translated ^{32}P-labeled pYT103. Crude mapping was performed by successive rehybridization of the same filter with different ^{32}P-labeled restriction fragments from pYT103 and pYT101 (14) (see Fig. 3C). To remove bound labeled probes, the filter was soaked in 0.4 N NaOH at 42°C for 30 min and washed in 0.1× SSC (1× SSC is 0.15 M NaCl plus 0.015 M sodium citrate)–0.1% sodium dodecyl sulfate–0.2 M Tris hydrochloride (pH 7.5) at 42°C for 30 min. One-dimensional (alkaline) and two-dimensional exonuclease VII analyses (neutral in the first direction, alkaline in the second) (K. Ozawa, J. Ayub, and N. Young, manuscript in preparation) were similarly performed by modification of the method described by Sharp et al. (34). To avoid interference with enzymatic digestion by formation of a hairpin structure during hybridization, the DNA probes were prepared by digestion of pYT103 with *Xba*I or *Aat*II to remove the inverted repeat sequence on the left side (the greater part of the right side repeats were not present in pYT103). Enzymatic digestion was accomplished by the addition of 300 μl of reaction buffer (30 mM KCl, 10 mM Tris hydrochloride [pH 8.0], 10 mM EDTA, 1 mM dithiothreitol, 20 U of single-stranded DNA of exonuclease VII [Bethesda Research Laboratories] per μg) to RNA-DNA hybrids in 30 μl of 80% formamide for 1 h at 37°C. Protected fragments were detected by Southern analysis. Precise S1 nuclease mapping was accomplished by hybridization of RNA with radioactively end-labeled probes derived from pYT103. The 5′ end was labeled with T4 polynucleotide kinase after dephosphorylation with alkaline phosphatase (Boehringer-Mannheim Biochemicals, Indianapolis, Ind.). Strand-specific 5′-end-labeled probes were obtained by restriction enzyme digestion, separation by agarose gel electrophoresis, and electroelution. Probes labeled at the 3′ end were prepared by a filling or exchange reaction with *Escherichia coli* DNA polymerase I Klenow fragment or T4 DNA polymerase (Bethesda Research Laboratories); strand-specific probes were produced by use of ^{32}P-labeled deoxynucleotides selected on the basis of the sequence of the ends of the template (22). S1 nuclease-protected fragments were resolved by 5 or 8% polyacrylamide–7 M urea gel electrophoresis. RNase protection mapping was done by the method described by Melton et al. (23) with [^{32}P]CTP for uniform labeling of probes. Various fragments of pYT103 were subcloned into pTZ18R and pTZ19R vectors (Pharmacia Fine Chemicals, Piscataway, N.J. [Div. Pharmacia, Inc.]), and RNA probes were prepared by in vitro transcription with T7 RNA polymerase (Pharmacia). Primer extension was performed by the method described by Treisman et al. (38). The 5′-end-labeled small fragments derived from pYT103 were used as primers. RNA-DNA hybrids were dissolved in 100 μl of reaction buffer (100 mM KCl, 60 mM Tris hydrochloride [pH 8.3], 6 mM $MgCl_2$, 5 mM dithiothreitol, 0.5 mM deoxynucleoside triphosphate, 0.8 U of RNasin per μl) to which was added 60 U of avian myeloblastosis virus reverse transcriptase (Life Sciences Inc., St. Petersburg, Fla.). After 1 h of incubation at 41°C, samples were extracted with phenol-chloroform, ethanol precipitated, and resolved by 5% polyacrylamide-urea gel electrophoresis.

Vector construction, transfection, and CAT assay. For detection of promoter function, vectors containing the chloramphenicol acetyltransferase (CAT) gene were made by using a pUC9 vector (Bethesda Research Laboratories) and a CAT cartridge (Pharmacia) linked to selected restriction enzyme fragments of pYT103. Frameshift mutants were made by restriction enzyme digestion of constructs followed by a filling reaction with the Klenow fragment of DNA polymerase I and recircularization by ligation (22). These constructs were introduced into HeLa cells by $CaPO_4$ transfection or into human erythroid bone marrow cells, which were cultured overnight in the presence of erythropoietin, by electroporation (29). At 48 h after transfection, CAT activity was assessed by the method described by Gorman et al. (16). Cell lysates were incubated with [^{14}C]chloramphenicol and acetyl coenzyme A for 1 h for HeLa cells and for 2 h for bone

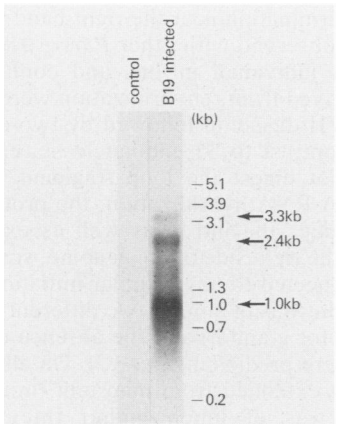

FIG. 1. Northern analysis. RNA was extracted from uninfected (control) or B19-infected total bone marrow cells, and 3 μg of total RNA was applied to each lane of a 1.5% formaldehyde gel. Samples were hybridized with ^{32}P-labeled pYT103 after transfer to nylon paper.

marrow cells. [^{14}C]chloramphenicol and its acetylated derivatives were separated by thin-layer chromatography.

RESULTS

B19 RNA transcription in limited numbers of erythroid cells. Inoculation of human erythroid bone marrow suspension cultures with B19 parvovirus results by days 7 to 10 in a dramatic decline in the proportion of morphologically recognizable erythroid cells (Ozawa et al., Blood, in press) that are associated with replication of B19 DNA (26). By in situ hybridization under nondenaturing conditions, in which both RNA and single-stranded DNA would be anticipated to hybridize with the probe, B19 was detected in a minority of the total cells in infected cultures and in about 30 to 40% of erythroid cells, which were fractionated by panning with anti-leukocyte antibodies (Ozawa et al., Blood, in press). With RNase A treatment before hybridization, the number of grains per cell was markedly decreased, indicating that most of the positive signal was due to the presence of B19 RNA (data not shown). The combination of RNase and S1 nuclease treatment completely abrogated hybridization. The number of cells with detectable B19 RNA was similar to the proportion expressing B19 capsid protein (Ozawa, et al., Blood, in press).

B19 RNA transcript species, splicing, and polyadenylation. RNA extracted from virus-infected cells 48 h after inoculation was subjected to Northern analysis (Fig. 1). Three broad major bands of 3.3, 2.4, and 1.0 kb (in ascending order of abundance) were detected with a B19-specific probe. Multiple RNA species were resolved by S1 nuclease analysis, employing a full-length B19 probe (pYT103 insert DNA), in neutral and alkaline gels (5); the neutral gels allowed the determination of transcript length, and the alkaline gels allowed the determination of exon length. In neutral gels, five transcripts of 3.1, 2.3, 2.2, 0.8, and 0.65 kb were apparent (Fig. 2A). [Because of the digestion of poly(A) tails by S1 nuclease, the size of the transcripts was slightly smaller than that determined by Northern analysis.] Under alkaline conditions, the 2.2-kb band was replaced by two new bands of 1.95 and 0.3 kb, indicating the presence of at least one spliced species (Fig. 2B). The decreased intensity of the 2.3-kb band on alkaline electrophoresis suggests that it, too, may have been partly spliced. (The 0.2-kb band was too faint for detection in alkaline gels.)

Spliced and unspliced RNA transcripts were discriminated by two-dimensional S1 nuclease analysis. By this method, protected fragments migrate by transcript size in the first, neutral dimension and then are further separated into exons in the perpendicular, alkaline dimension (15). Eight transcripts were apparent by use of this procedure (Fig. 2C). Four RNA species were clearly spliced: c was composed of exons of 0.3 and 1.95 kb; d was composed of exons 0.2 and 1.95 kb, g was composed of exons of 0.3 and 0.3 kb; and h was composed of exons of 0.2 and 0.3 kb. The remaining four RNA species (a, b, e, and f) lay along the diagonal of the two-dimensional gel. Two of the smallest species (e and f), however, were slightly displaced from the diagonal, suggesting the possible presence of a small additional exon. An almost probe-length band or spot was occasionally present on both one- and two-dimensional gels. Because transcripts of this size were not detected by Northern analysis, they may have represented artifacts; if authentic, such a full-length transcript would be a very minor RNA species.

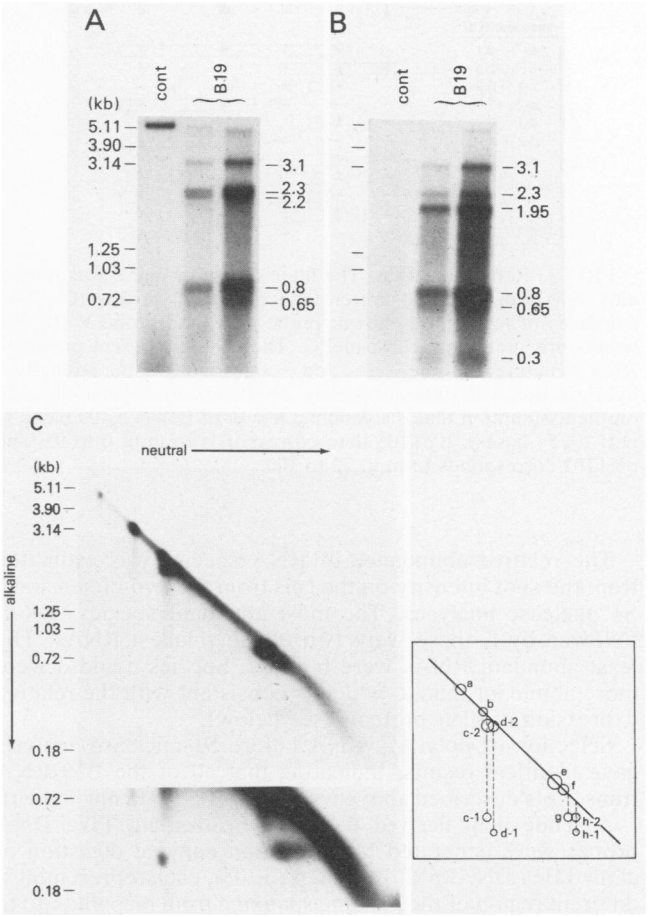

FIG. 2. S1 nuclease analysis of B19 transcripts with a full-length B19 DNA probe (pYT103 insert). Total RNA (5 μg) from uninfected bone marrow cells (control [cont]) or 0.5 μg (left lane) and 2 μg (right lane) from the B19-infected samples were hybridized with 0.1 μg of pYT103 DNA. S1 nuclease-protected fragments resolved by neutral (A) or alkaline (B) 1.5% agarose gel electrophoresis followed by Southern transfer and hybridization with ^{32}P-labeled pYT103 probe. (C) Two-dimensional S1 nuclease analysis of 3 μg of total RNA from infected bone marrow cultures. The lower portion of panel C shows a longer exposure of part of the upper portion of panel C. The diagram indicates the location of transcripts and exons. (Spot size is shown in the diagram in Fig. 3C.)

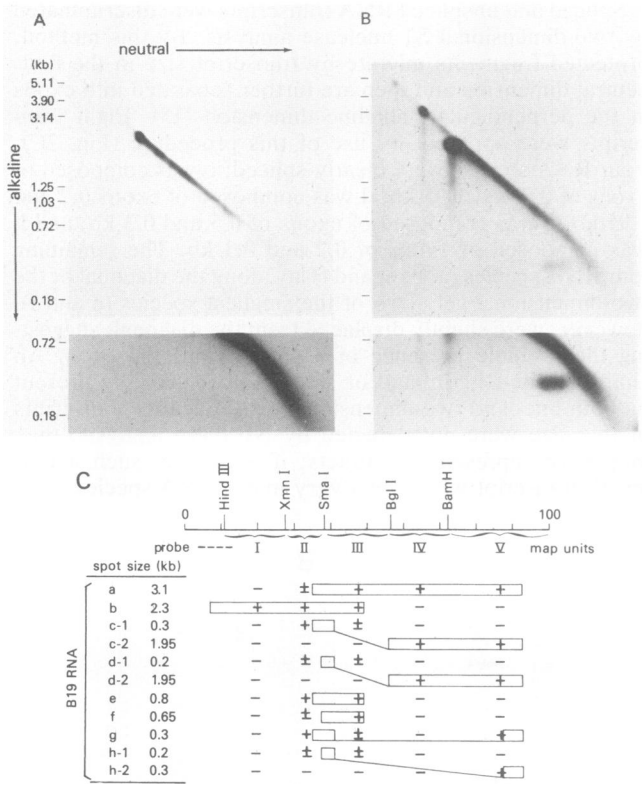

FIG. 3. Rehybridization. The filter shown in Fig. 2 was repeatedly rehybridized with shorter than full-length probes (C). Two examples of results are shown: probe I (A) and probe V (B). All results are summarized in panel C. The boxes represent predicted RNA structure; and the +, ±, and − signs indicate the strength of hybridization with different probes. Map units are calculated based on the assumption that the genomic length of B19 is 5,400 bases (1 m.u. = 54 bases). pYT103 then corresponds to m.u. 0 to 95, and pYT101 corresponds to m.u. 72 to 100.

The relative abundance of RNA species was estimated from the spot intensity on the gels from the two-dimensional S1 nuclease analyses. The most abundant species was e, followed by f; these were two of the smallest RNAs. The least abundant RNAs were b and a. Species c and d were more abundant than a, which is consistent with the relative expression of their proteins (see below).

Selection of poly(A)$^+$ RNA before S1 nuclease analysis gave identical results, indicating that all of the B19 RNA transcripts described above were poly(A)$^+$ (data not shown).

A crude map derived from rehybridization. Five DNA probes were generated by restriction enzyme digestion of cloned B19 DNA (pYT101 and pYT103), each representing a different region of the genome spanning from map units 10 to 100 (Fig. 3). The probes were used to analyze two-dimensional S1 nuclease gels by successive rehybridization of the same filter. Representative results for two of the probes are shown in Fig. 3A and B. The far left-hand probe (I) detected only the single RNA species b of 2.3 kb (Fig. 3A). The far right-hand probe (V) detected five transcripts (3.1 kb of a, the 1.95-kb exons of c2 and d2, and two different 0.3-kb exons from g and h2; Fig. 3B). The summary of all hybridizations is shown in Fig. 3C. These results suggest that three B19 RNA species (b, e, and f) terminated in the middle of genome, which is in contrast to the consistent pattern of cotermination near the right-hand terminus for all RNA species observed with other *Parvoviridae*.

The size of individual introns and confirmation of the crude map derived from rehybridization were obtained from exonuclease VII digestion followed by two-dimensional gel analysis. In contrast to S1 endonuclease, exonuclease VII enzyme did not digest the loop fragment formed by the intron on DNA-RNA hybridization; the protected fragment therefore includes the intron as well as exons. From the crude map of the right side of the genome, species, a, c, d, g, and h were expected to have similar initiation and termination sites; but introns of at least two different sizes (small for c and d, large for g and h) and the absence of an intron for transcript a were predicted (Fig. 3C). On alkaline gels with the probe that extended from map unit (m.u.) 9 to 95, the 3.1-kb band was of much higher intensity following exonuclease VII digestion than following S1 nuclease digestion, suggesting that these five species overlap (Fig. 4Aa). Overlapping was demonstrated by the separation of the 3.1-kb species into three groups on two-dimensional gels; the three discrete spots probably corresponded to species a, c-d, and g-h (Fig. 4Ba).

Precise mapping. To more exactly determine the location of the borders of the various exons, multiple small restriction enzyme fragments were prepared based on the results of crude mapping. These fragments were used as probes after radioactive labeling at the 5′ or 3′ ends in S1 nuclease protection analysis (Fig. 5). In the case of the least-abundant transcript (b), which was not detectable by using end-labeled probes, conventional S1 nuclease analysis described by Berk and Sharp (5) (Fig. 5D) or RNase protection analysis (see below) were employed. Map units 6; 35 and 37.5; 56; and 87 were analyzed for 5′ borders of exons and map units 40.5, 49, and 92.5 were analyzed for the 3′ borders (Fig. 5A). Representative autoradiographs are shown in Fig. 5B and C for 5′ and 3′ probes, respectively. That all transcripts were detected with strand-specific probes confirms that only the minus DNA strand of the virion serves as a template for RNA transcription, as predicted from the open reading frames based on the nucleotide sequence (33).

The 3′ border of exons at m.u. 92.5 were located just downstream of a polyadenylation signal at nucleotide 4990, which was predicted from the sequence of B19 (33). The 3′ border of exons at m.u. 49 coincided with unusual polyadenylation signals at nucleotide 2639 (ATTAAA) and at nucleotide 2645 (AATAAC). The unchanged size of the 0.8-kb fragment protected by probe a following exonuclease VII analysis supported termination at this point rather than the presence of a large right-side intron and termination of transcripts b, e, and f at the conventional m.u. 92.5 polyadenylation site (Fig. 4Aa). However, this method may not be sufficiently sensitive to detect splicing of transcripts to a very small (<50 nucleotides) far right-hand exon (see discussion).

Multiple TATA-like sequences were observed in the nucleotide sequence of B19 (33). However, only the far left-side promoter at about m.u. 6 was compatible with the 5′ border of RNA transcript b. In contrst, there were no appropriately located promoterlike sequences proximal to the 5′ borders of transcripts at m.u. 35 and 37.5. The nearest upstream TATA sequence was almost 700 nucleotides distant; other nearby promoterlike sequences were located within the transcription unit.

Most B19 transcripts have short leader sequences. The absence of appropriately placed promoters for many of the right-side transcripts suggests the presence of exons at the

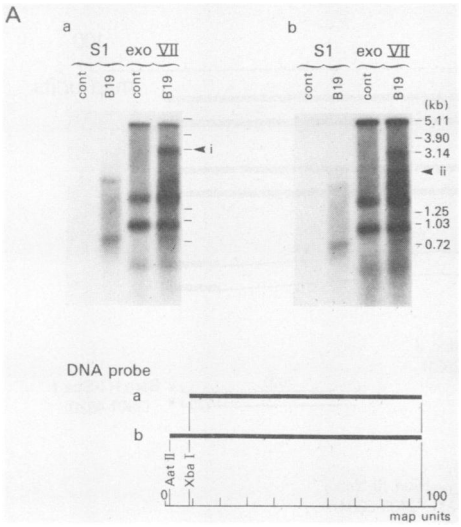

FIG. 4. Exonuclease VII analysis. RNA-probe DNA hybrids were digested with exonuclease VII, which, in contrast to S1 nuclease, does not cleave within introns. (A) Alkaline gel electrophoresis of protected fragments of the two probes a and b are shown. Filters were hybridized with ^{32}P-labeled pYT103 after Southern transfer. Similar RNA quantities (2 μg) and exposure times were used for comparable S1 nuclease and exonuclease VII experiments. Exonuclease VII digestion resulted in the appearance of a dense band at 3.1 kb (arrow at i) by using probe a; another new band appeared at 2.3 kb (arrow ii) by using probe b. (Longer exposure of the filter showing S1 nuclease digestion results [A] led to a pattern similar to that shown in Fig. 2B. Bands in control [cont] lanes for exonuclease VII analysis were artifacts of the enzymatic digestion due to the secondary structure of the probes.) (B) Two dimensional exonuclease VII analysis allowed separation of the components of the dense 3.1- and 2.3-kb bands seen on one-dimensional gels, as well as discrimination of hybrids of probe length. Probe a was used in panel a, and probe b was used in panels b and c. (a) Three different spots (arrowheads) were observed at 3.1 kb. (b) A new spot appeared (large arrowhead) when hybridization was done with probe b. Three faint spots were seen at about 4.7 kb; this is clearer in the longer exposure of the inset (arrowheads). (c) Control RNA from uninfected cells.

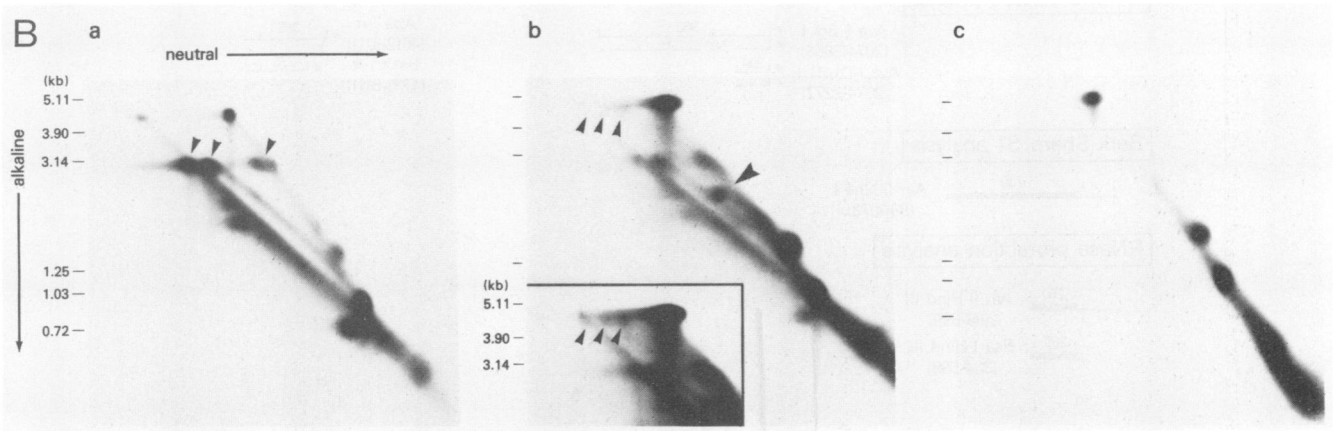

far left side of the genome, which is too short to be detectable by two-dimensional S1 nuclease analysis by the Southern transfer technique. The presence of short leader sequences was inferred from results of primer extension experiments. Results showing comparisons of primer extension and S1 nuclease analyses are shown in Fig. 6. One example of the interpretation of these experiments is given for the a, a′, e, and f transcripts. In S1 nuclease analysis with the 5′-end-labeled *Hin*dIII-*Tth*111I probe (nucleotides 1538 to 2277), two protected fragments of 370 and 250 nucleotides were generated. Primer extension with a 5′-end-labeled probe (*Ava*I-*Tth*111I; nucleotides 2076 to 2277) resulted in two different sizes of the reverse transcripts (430 and 305 nucleotides), both of which were about 50 to 60 nucleotides longer than the S1 nuclease-protected fragments. Similar differences of about 50 bases were found for all the RNA species examined (c, d, g, and h, as well as a, a′, e, and f).

The location of these 50- to 60-nucleotide exons was established by exonuclease VII analysis. Following hybridization and enzymatic digestion, disparate results were obtained with the *Xba*I–right-hand end (m.u. 8.9 to 94.6) probe and a slightly longer, almost full-length probe (*Aat*II–right-hand end; m.u. 1.7 to 94.6) (Fig. 4A and B). On alkaline gels, experiments with the longer probe (Fig. 4Ab) resulted in the appearance of a heavy band at 2.3 kb that was separable on two-dimensional gels into two spots that were strikingly different in their intensities (Fig. 4Bb). The denser spot likely represented the major transripts e and f; the lighter spot likely represented the most minor transcript b.

Similarly, the presence of short 5′ exons for transcripts which terminated at the right end (a, c, d, g, and h) were predicted to result in exonuclease VII-protected fragments that were approximately the same size as the probe (*Aat*II–right-hand end). On one-dimensional gel analysis, these could not be discriminated from reannealing of the probe (Fig. 4Ab). In two-dimensional analysis with the longer probe, however, three spots at 4.7 kb that were slightly shorter than the probe length of 5 kb were apparent, probably corresponding to transcripts a, c and d, and g and h (Fig. 4Bb). Neither the 4.7-kb nor 2.3-kb multiple spots were observed with hybridization by using the slightly shorter *Xba*I probe (Fig. 4Aa and Ba). The short exons for all transcripts were therefore localized to the region between m.u. 1.7 and 8.9.

Further confirmation of the short 5′ exon in ths region was obtained by RNase protection analysis with a uniformly labeled RNA probe corresponding to the restriction fragment *Aat*II-*Hin*dIII (nucleotides 88 to 599) (Fig. 7). An apparent protected fragment of about 60 bases was present, as was the larger protected fragment (about 260 nucleotides) derived from minor transcript b. By using several different

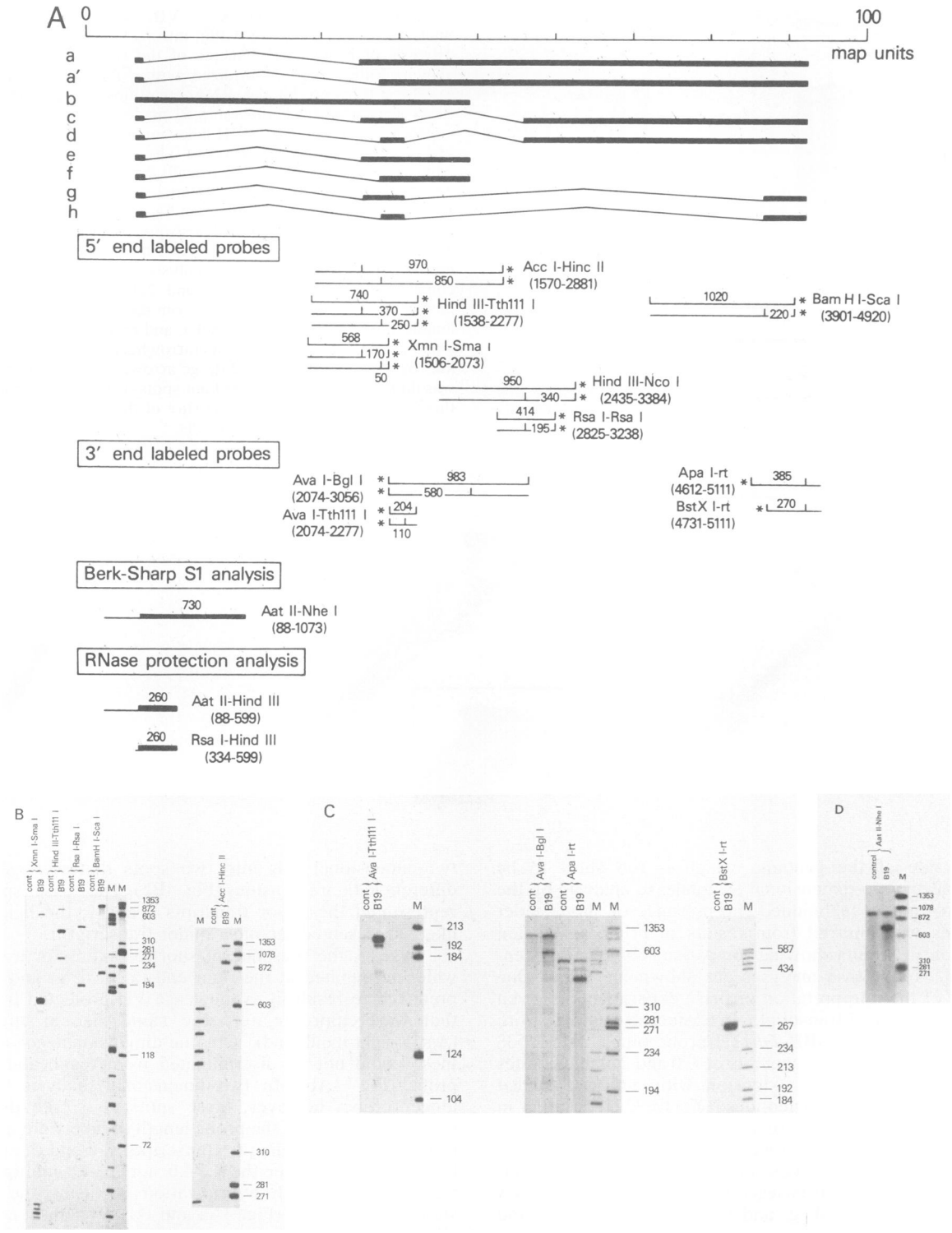

FIG. 5. Precise S1 nuclease mapping of exon boundaries. (A) Probes employed for precise mapping of the 5′ and 3′ exon boundaries and their protected fragment sizes are shown below the B19 transcription map. (B) Representative data from S1 nuclease analysis with 5′-end-labeled probes. Probe *Xmn*I-*Sma*I was used to determine the 5′ boundaries of transcripts a, a′, c, d, e, f, g, and h. Protected fragments of 170 nucleotides suggested that m.u. 35 is the major 5′ border of the second exons and fragments of 50 nucleotides suggested that m.u. 37.5 is the minor 5′ border of these exons. For probe *Hin*dIII-*Tth*111I (for transcripts a, a′, e, and f), protected fragments of 370 and 250 nucleotides suggested that m.u. 35 and 37.5 are the major and minor 5′ borders of the second exons, respectively. For probe *Rsa*I-*Rsa*I (for transcripts c and d), the protected fragment of 195 nucleotides suggested that m.u. 56 is the 5′ border of the third exons. For probe *Bam*HI-*Sca*I (for transcripts g and h), a fragment of 220 nucleotides suggested that m.u. 87 is the 5′ border of the third exons. For probe *Acc*I-*Hin*cII (for transcripts a and a′), protected fragments of 970 and 850 (faint) nucleotides suggested that m.u. 35 and 37.5 are major and minor 5′ borders

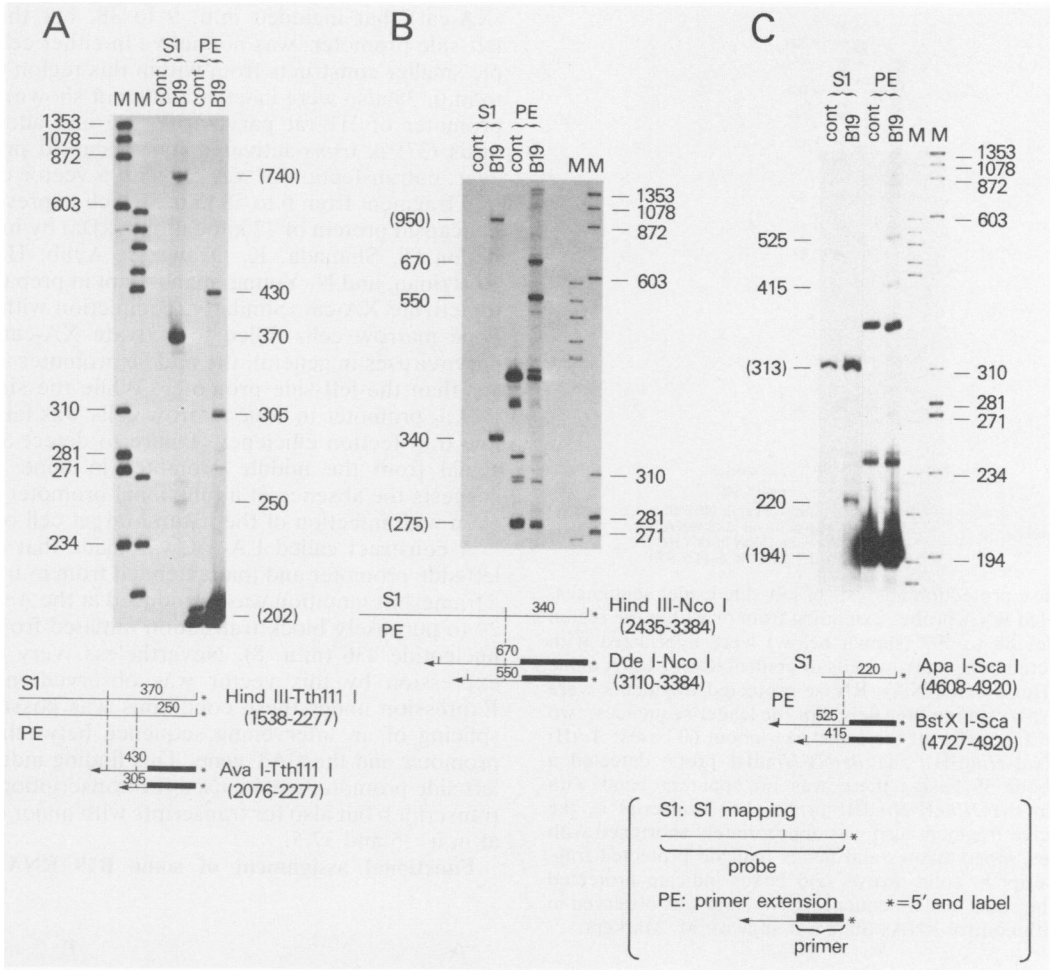

FIG. 6. Primer extension (PE) analysis. This method was used to demonstrate short leader sequences or exons by comparison with S1 nuclease-protected fragments. Abbreviations: cont, Control; M, markers. (A) For transcripts a, a′, e, and f, a fragment from nucleotide 1538 to 2277 was used for S1 nuclease protection experiments, and a much shorter fragment (nucleotides 2076 to 2277) was used as a primer to generate reverse transcripts. The reverse trnscripts were 50 to 60 nucleotides longer than the S1-protected fragments, which is consistent with the presence of a short leader sequences. Although transcripts a and a′ were much less abundant than transcripts e and f, the same-sized bands observed with S1 nuclease-protected fragments were not seen even with much longer exposures. (B) For transcripts c and d, S1 nuclease analysis was done with fragments 2435 to 3384; primer extension was done with fragments 3110 to 3384. S1 nuclease analysis showed a single fragment that was 340 nucleotides from the far right side of the main exon. Primer extension analysis showed two larger fragments (670 and 550 nucleotides) that were probably derived from the third exon (340 nucleotides), the second exon (275 or 155 nucleotides), and the far left side first exon (50 to 60 nucleotides). (C) For transcripts g and h, S1 nuclease analysis was done with fragments 4608 to 4920, primer extension was done with fragments 4727 to 4920. Results are comparable to those described above (see panel B). Bands which appeared in both control and infected lanes were considered artifacts of the primer extension reactions, because they also appeared on the addition of tRNA alone.

restriction fragments from this region, leader sequences were localized to lie between nucleotides 340 and 410. This result implicates the TATA sequence at nucleotide 319 as a functional promoter. In addition, this site corresponded to the 5′ exon border of the single, unspliced transcript b, suggesting the common origination of all B19 transcripts at m.u. 6.

Splicing donor and acceptor sites. Splice sites could be predicted from the results of S1 nuclease analysis and RNase mapping and from the B19 DNA nucleotide sequence (33).

of second exons, respectively. cont, Control. (C) Autoradiographs from S1 nuclease analysis with 3′-end-labeled probes. For probe *Ava*I-*Tth*111I (for probes c, d, g, and h) only the protected fragment of 110 nucleotides is consistent with the initial crude mapping data and suggested that m.u. 40.5 is the 3′ border of the second exons. The two bands smaller than probe size may be artifactual, possibly due to sequence mismatching between parvovirus in Minor II serum and the pYT103 DNA. For *Ava*I-*Bgl*I (for transcripts b, e, and f), protected fragment of 580 nucleotides suggested that m.u. 49 is the 3′ border of the first exon of b and the second exon of e and f transcripts. For probe *Apa*I-right end (for transcripts a, a′, c, and d), a protected fragment of 385 nucleotides suggested that m.u. 92.5 is the 3′ border of the second exons of a and a′ and the third exons of c and d transcripts. For the probe *Bst*XI-right end (for transcripts g and h), protected fragment of 270 nucleotides suggested that m.u. 92.5 as the 3′ border of the third exons. (D) S1 nuclease analysis for transcript b by the method described by Berk and Sharp (5). Fragment *Aat*II-*Nhe*I was hybridized with RNA samples, and S1 nuclease-protected fragments were resolved by Southern transfer and hybridization with ^{32}P-labeled pYT103. The protected fragment of 730 nucleotides suggested that m.u. 6 is the 5′ border of the exon. (RNase mapping is shown in Fig. 7.)

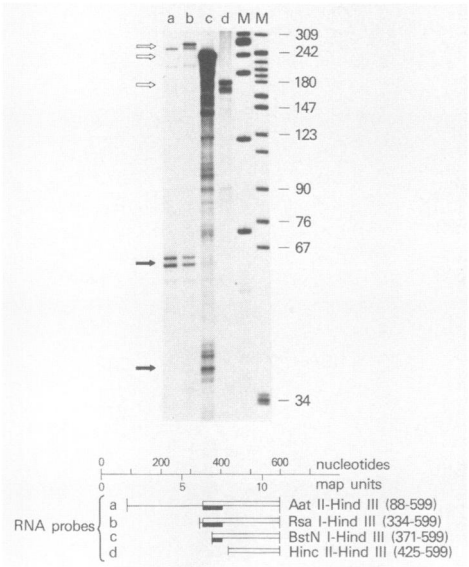

FIG. 7. RNase protection analysis of left-side leader sequences. Uniformly labeled RNA probes extending from or within the region from nucleotides 88 to 599 (shown below) were hybridized with RNA from infected bone marrow cells or control RNA (tRNA alone or uninfected HeLa cell RNA). RNase-protected fragments were resolved in polyacrylamide-urea gels. For the leader sequences, two probes detected fragments of the same size (about 60 bases; *Aat*II-*Hin*dIII and *Rsa*I-*Hin*dIII); the *Bst*NI-*Hin*dIII probe detected a fragment of about 35 bases; there was no apparent band with hybridization to the *Hinc*II-*Hin*dIII probe. For transcript b, the 260-base-protected fragment also was appropriately shortened with the same probes. Open arrows and boxes indicate protected fragments of transcript b, solid arrows and boxes indicate protected fragments for the short leader sequences. No band was observed in experiments with control RNAs (data not shown). M, Markers.

This analysis was predicated on the use of consensus sequences (GT for donor sites and AG for acceptor sites). Although it is almost universally employed, an exception in parvoviruses has been reported (GC for GT in the large intron splice of MVM; 18).

The splicing donor site (GT) for the short leader sequences was available at nucleotides 407 and 408. For the acceptor site, a single AG sequence was located at nucleotides 1908 and 1909 at about m.u. 35, implying that the 5′ exon border is nucleotide 1910. For the boundary at m.u. 37.5, a single AG is located at nucleotides 2028 and 2029. Four splicing donor sites were possible between nucleotides 2177 and 2195 at m.u. 40.5, the use of which in vivo could not be discriminated by S1 nuclease analysis. Two acceptor sites were also possible at m.u. 56 (nucleotides 3043 and 3044, and 3049 and 3050) and at m.u. 87 (nucleotides 4702 and 4703, and 4708 and 4709).

A left-side promoter (p_6) for B19 transcription. The transcription map suggests that all B19 transcription is driven from a left-side promoter at about m.u. 6. In addition, there was little evidence of initiation of transcription in the middle of the genome from an internal promoter, which is characteristic of other animal parvoviruses. Functional promoter assays were performed by using vectors constructed from various putative B19 promoter sequences linked to the CAT gene to test this hypothesis (Fig. 8). A construct including the far left side of the genome (m.u. 0 to 7; LB-cat) expressed CAT efficiently in HeLa cells, and CAT activity was detectable in fresh erythroid bone marrow. A construct (XA-cat) that included m.u. 9 to 38, but that lacked the left-side promoter, was not active in either cell type. Multiple smaller constructs from within this region that extended to m.u. 38 also were inactive (data not shown). The internal promoter of H1 rat parvovirus (31) and adeno-associated virus (37) is *trans*-activated by noncapsid proteins. However, cotransfection of XA-cat with a vector containing the B19 fragment from 0 to 58 m.u., which expressed the major noncapsid protein of 77 kilodaltons (kDa) by immunoprecipitation (T. Shimada, K. Ozawa, J. Ayub, H. Yu-Shu, G. Kurtzman, and N. Young, manuscript in preparation), failed to activate XA-cat. Similarly, coinfection with B19 virus of bone marrow cells failed to activate XA-cat. For animal parvoviruses in general, the middle promoter appears stronger than the left-side promoter. While the signal from the B19 p_6 promoter in bone marrow cells was faint, due to the low transfection efficiency, failure to detect a concomitant signal from the middle promoter in bone marrow cells suggests the absence of a functional promoter in this region even with infection of the natural target cell of the virus.

A construct called LA-cat was made that contained the left-side promoter and that extended from m.u. 0 to m.u. 38; a frameshift mutation was introduced at the *Acc*I site at m.u. 29 to purposely block translation initiated from the ATG at nucleotide 436 (m.u. 8). Nevertheless, very efficient CAT expression by this vector was observed in HeLa cells. Expression under these conditions was possible only with splicing of an intervening sequence between the left-side promoter and the CAT gene. This finding indicates that the left-side promoter can be used for transcription, not only for transcript b but also for transcripts with major exons starting at m.u. 35 and 37.5.

Functional assignment of some B19 RNA species. For

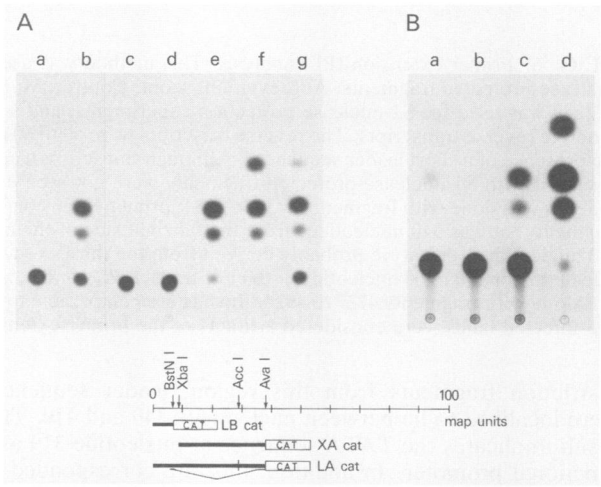

FIG. 8. Promoter function in a transient CAT expression assay. Vectors were constructed to include putative promoter sequences from the B19 genomic sequence (33), linked to the CAT gene, and transfected by calcium phosphate-mediated transfer into HeLa cells (A) or by electroporation into human erythroid bone marrow cells (B). (A) Lane a, pUC-9 control; lane b, LB-cat, which included a left-side promoter; lane c, XA-cat, including upstream sequences of the middle exons, excluding the far left-side promoter; lane d, cotransfection of XA-cat with a vector that expressed the major noncapsid protein of 77 kDa (m.u. 0 to 58); lane e, LA-cat, which comprises m.u. 0 to 38, contained the left promoter and a frameshift mutation at m.u. 29; lane f, pRSV-cat, positive control CAT vector; lane g, enzyme control. (B) Lane a, LB-cat; lane b, XA-cat; lane c, pRSV-cat, all coinfected with B19; lane d, enzyme control.

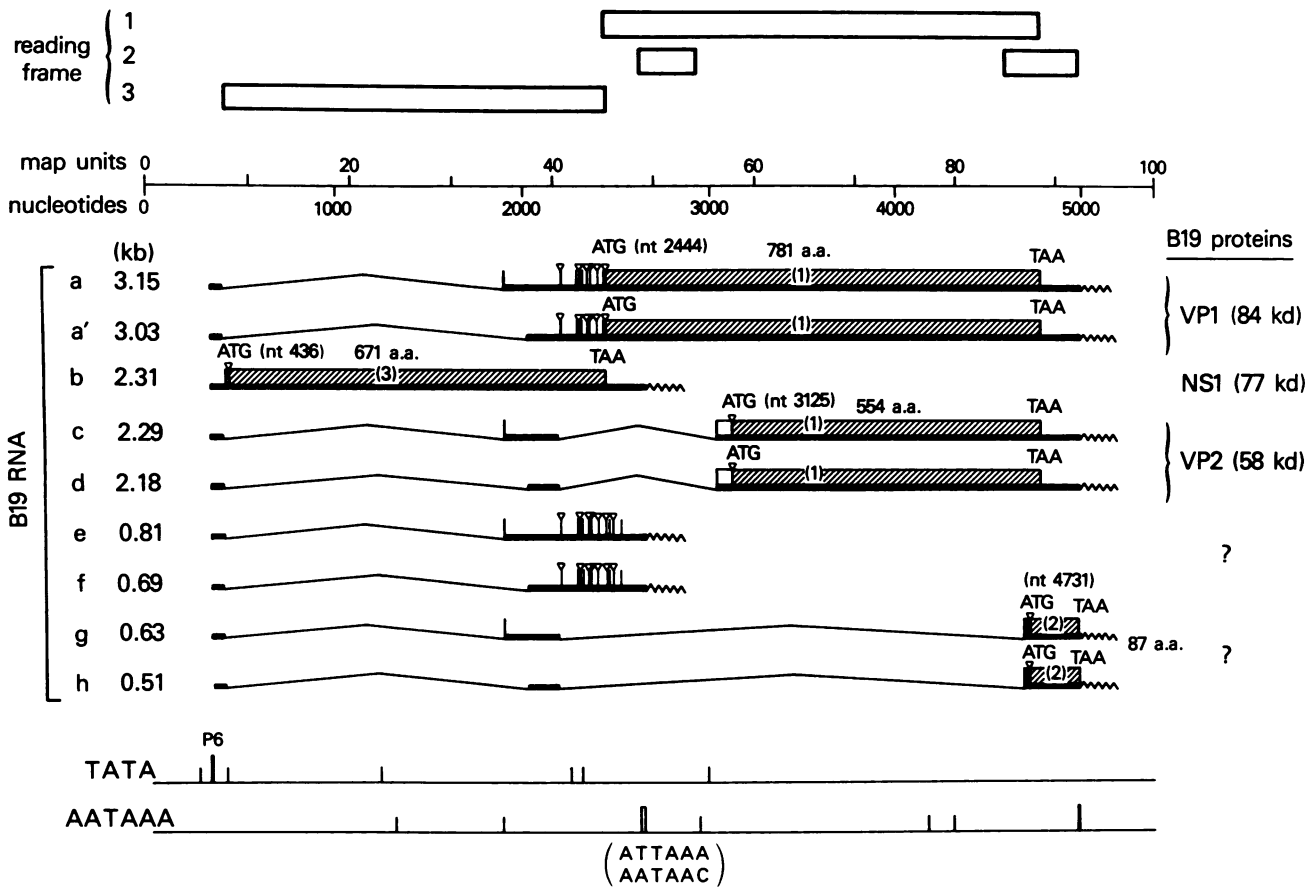

FIG. 9. Transcription map of B19 parvovirus. Transcripts are in order by length. Shown is the location of the p_6 promoter, functional polyadenylation signals, splice donor and acceptor sites, open reading frames (boxes), ATG sequences (vertical lines), purine-NNATG (consensus sequence described by [20]; open triangles), and translation initiation and termination sites (defined by the limits of the shaded areas of boxes showing open reading frames). Frame numbers are indicated within the boxes. For the TATA sequences, the bold line indicates the functional promoter, and the thin lines indicate other, nonfunctional TATA regions. Similarly, for potential polyadenylation signals, the solid bold line indicates the functional conventional site, the open line indicates the variant and functional polyadenylation site, and the thin lines indicate nonfunctional AATAAA sequences.

transcript b, the first ATG occurs at nucleotide 436, within a consensus sequence described by Kozak (20) (purine-NNATG). From the results of the construction of vectors containing B19 sequences and their mutants and analysis by immunoprecipitation of B19-specific proteins after transfection into HeLa cells, the 77-kDa major noncapsid protein could be assigned to transcript b (Shimada et al., manuscript in preparation). The ATG at nucleotide 436 in reading frame 3 represented the translation starting codon for this protein (Fig. 9).

The B19 capsid proteins are encoded by the right side of the genome (13). The 84-kDa capsid protein would be predicted to be encoded by transcripts a and a'. The sixth ATG sequence (located at nucleotide 2444) in a sequence described by Kozak (20) in reading frame 1 is probably used, because the first five ATGs are followed shortly by in-frame termination codons. The 58-kDa major capsid protein is probably encoded by transcripts c and d. The ATG codon at nucleotide 2444 is spliced out, and the first appropriate ATG codon at 3125 in reading frame 1 is probably employed.

Proteins corresponding to other RNA species have not been identified. The function of the most abundant transcripts e and f is puzzling, because no appropriate ATG codon is located within either the leader sequence or the main exon. It is possible that B19 employs an unusual initiation codon, like the threonine codon ACG that initiates translation of capsid protein B by adeno-associated virus-2 (3). Use of an ACG codon located at nucleotide 2062 could generate a protein product of 129 amino acids from frame 3. Transcripts g and h may initiate translation of proteins of about 90 amino acids from ATGs at nucleotides 4710 or 4731 in frame 2, depending on the selection of splicing sites.

The transcription map of B19, including the functional promoter site, polyadenylation signals, splice sites, and open reading frames, is shown in Fig. 9.

DISCUSSION

Despite distinct biological behaviors, the patterns of RNA transcription for the defective (adeno-associated virus) and autonomous parvoviruses are remarkable more for their similarity than for their differences (9) (Fig. 10). The B19 parvovirus shares many common features with other parvoviruses. As in the organization of the general parvovirus genome, the B19 structural or capsid proteins are encoded by the right half, and at least one of the B19

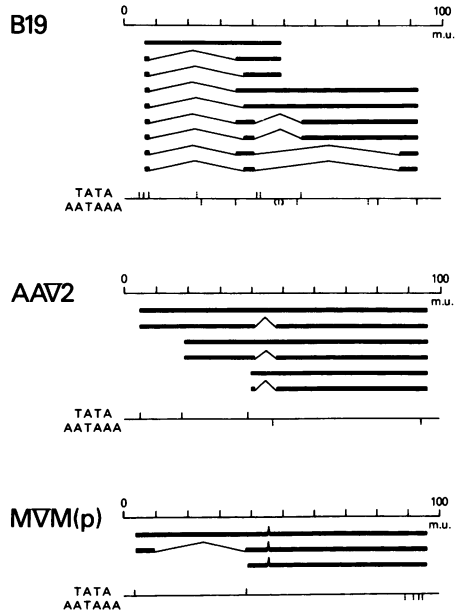

FIG. 10. Comparison of transcription map of B19 (rearranged for this purpose) with the maps of adeno-associated virus-2 (AAV2) (9, 36) and minute virus of mice (MVM) (18, 24). Solid vertical lines indicate functional, and dotted lines indicate nonfunctional TATA and AATAAA sequences. A varient polyadenylation signal is indicated in parentheses.

noncapsid proteins is encoded by the left half. To compensate for the extremely limited length of the genome, parvoviruses employ a variety of mechanisms to increase the coding potential of 5 kb of nucleotides: A pattern of overlapping RNA transcription results from extensive utilization of all three reading frames and the generation of multiple RNAs by splicing. The complexity of the B19 transcriptional map may represent the extreme example of these mechanisms. Based on their apparent electrophoretic size, the total number of transcripts in parvoviruses has ranged from three or four for autonomous rodent parvoviruses (18, 21, 24) to 6 for adeno-associated virus-2 (37) (use of alternate nearby splice donor and acceptor sites can generate larger numbers of transcripts, without apparent size differences, which are usually detected only after cDNA cloning [18, 24]). We identified at least nine B19 transcripts in RNA extracted from infected erythroid cells (the number may be larger, depending on variation in the use of splicing sites for some transcripts). Another full-length transcript was suggested on some S1 nuclease analytical gels.

For comparative purposes, the B19 RNA species were rearranged, as shown in Fig. 10. The genomic organization of adeno-associated virus and minute virus of mice is characterized by the presence of two classes of overlapped RNA transcripts, one spliced and the other unspliced (9). B19 shows such a trio of spliced and unspliced RNAs from the left half of the genome (b, e, and f). In addition, there are three sets of pairs: transcripts that almost span the B19 genome, composed of RNAs with a single long left side intron (a, a'); the left side intron and a short right-side intron (c, d); and the left-side intron and an even longer right-side intron (g, h). While the intron length in adeno-associated virus, a human but nonpathogenic parvovirus, is generally short, the length of many of the introns of B19 transcripts resembles that of the single RNA species (R2) with a long left-side intron produced by rodent parvoviruses. In B19, these long introns are associated for eight of nine RNAs with short (about 60-base) leader sequences. Such a short leader sequence has been described for the 2.3-kb capsid mRNA of adeno-associated virus-2, but the leader sequence of the 3.3-kb RNA (R2) of rodent parvoviruses is much longer (300 bases).

From the genomic sequence of B19 (33), many possible promoter sites were predicted. The autonomous parvoviruses have two promoters, one at the left side of the genome (p_{4-5}) for the noncapsid proteins and one internal (P_{38-40}) for the capsid proteins. Adeno-associated virus-2 has three functional promoters (p_5, p_{19}, and p_{40}). In B19, TATA sequences have been identified at m.u. 5 to 8, 23, 42 and 43, and 55; the fourth region, based on the position of a downstream ATG codon in an open reading frame, was thought likely to drive transcription of the major capsid protein mRNA (33). However, we found that all the putative promoter regions, except the far left-side TATA boxes, are located within transcription units. The transcription map shows that in their natural target cells, all B19 transcripts start at a single far left-side promoter located at m.u. 6 (p_6). In confirmation, only the left-side promoter could be demonstrated to be functionally active in transient CAT expression assays. In other parvoviruses, the strong internal promoter has been assumed to be more efficient than the left-side promoter, as reflected by the relative abundance of the capsid compared with noncapsid proteins (9). However, an internal promoter function in B19 could not be demonstrated even within erythroid cells, in which the left-side promoter function was detectable, or in the presence of possibly *trans*-activating noncapsid proteins.

The nucleotide sequence of B19 showed multiple potential polyadenylation signals (AATAAA) at m.u. 24, 35, 54, 77, 80, and 92 (33). An internal AATAAA sequence was present in adeno-associated virus-2 but not in the genomes of autonomous animal parvoviruses, although all transcripts from these parvoviruses coterminate at the far right side at polyadenylation sites at about m.u. 95. In contrast, three of the nine B19 transcripts appeared to terminate in the middle of the genome. These transcripts presumably use an unusual polyadenylation signal at m.u. 49 (ATTAAA or AATAAC) which was not predicted. These particular variant sequences have been reported rarely as a polyadenylation signal for eucaryotic genes (ATTAAA, used in 12% of transcripts, and AATAAC, used in 1% of transcripts [6, 41]) and associated with tissue specificity (44). That these variant polyadenylation signals are indeed functional has been suggested by results of experiments done in HeLa cells: When transfected with a plasmid containing sequences from the left side of the B19 genome (m.u. 0 to 53), which excludes the conventional polyadenylation signals from the right side of the genome, the same-size poly(A)$^+$ transcripts, corresponding to b, e, and f, were detected, as was the case in cells transfected with full-length pYT103 plasmid (unpublished data). Sequencing of cloned cDNA from infected erythroid cells will be required to confirm utilization of these unusual polyadenylation signals in the target cells of the virus.

Three to five protein products of B19 were identified. The two capsid proteins of 58 and 84 kDa (VP2 and VP1, respectively) are produced in infected human erythroid bone marrow cells in culture (27) and are present in virions and in infected human fetal tissue (13; N. Young and K. Ozawa, *in* J. R. Pattison, ed., *Parvoviruses and Human Disease*, in press). These two capsid proteins are analogous to the two

or three structural proteins of other parvoviruses in the similarity of their size and abundance. Like other parvovirus capsid proteins, the B19 capsid proteins are encoded by RNA transcripts from the right side of the genome, the major (>90% in capsid constitution and cell synthesis) 58-kDa protein (VP2) is encoded by the c and d transcripts, and the minor 84 kDa protein (VP1) is encoded by the a and a' transcripts. Additionally, the major noncapsid protein of 77 kDa (27) was encoded by the mRNA b, as determined by promoter deletion and frameshift mutation experiments (Shimada et al., manuscript in preparation). Assignment of the two minor noncapsid proteins (52 and 34 kDa [27]), which could represent degradation products or proteins that have undergone posttranslational modification, to specific mRNAs is more problematic. The functional role of many of the B19 RNA species is unknown; two of these species, e and f, are the most abundant RNAs transcribed.

The coding capacity for several abundant transcripts (e, f, g, and h) is quite limited, although they could encode for low-molecular-weight proteins which have not been detected to date. The origin of these RNAs from defective interfering particles (8) is highly unlikely for several reasons: There is no evidence for significant amounts of B19 DNA of other than full genomic length in infected cells (26) and parvovirus-defective particles contain large internal deletions (8). More interesting is the possibility that these RNAs have regulatory functions, similar, for example, to adenovirus virus-associated (VAI) RNA, which increases translation by preventing inactivation of eucaryotic initiation factor 2 (32), or to small nuclear RNAs, designated U1 to U6, which are required for RNA processing (4). However, no significant homology was detected between the appropriate region of the B19 genome spanning nucleotides 1910 to 2655 and either the human U1 gene (40% homology by alignment but over many short sequences) or the 5' end of the VAII gene of adenovirus 5 (20% homology). Determination of both of these regions was done with a MicroGenie (Beckman Instruments, Inc., Palo Alto, Calif.).

Computer analysis of the nucleotide sequence suggests that B19 shares properties with both major genera of the *Parvoviridae*, but that B19 is as separate evolutionarily from autonomous rodent and nonpathogenic human adeno-associated viruses as these viruses are from each other (33). For example, B19 shares a similarity in its 5' and 3' terminal hairpin structures like adeno-associated virus, although it behaves as an autonomous virus in culture (43; Ozawa et al., Blood, in press). Also, both B19 and adeno-associated virus lack the conserved regions of the right open reading frame common to autonomous parvoviruses (10, 33). We have shown here that the transcription map of B19 also diverges markedly from the maps of both the defective and autonomous parvoviruses. Possibly, all three types of virus evolved from a common ancestor (perhaps a protoparvovirus with a left-side promoter and a single transcription unit). Alternatively, B19 may have evolved from an adeno-associated virus-like parvovirus through the loss of internal promoter function and a gain in RNA complexity. The vestigial presence of nonfunctional internal TATA sequences and the structural similarities to adeno-associated virus within the B19 genome would favor the latter hypothesis.

With only a single functional promoter, B19 transcript abundance cannot be regulated by differential promoter strength or *trans*-activation by noncapsid proteins of one of several promoters. In other parvoviruses, the use of alternate splicing patterns may regulate the differential expression of capsid and noncapsid proteins (9). B19 must rely on splicing events, pausing or termination in the middle of transcription, or polyadenylation signal recognition to control the quantity of the different RNAs that are produced. An unusual transcriptional strategy may underlie autonomous phenotype and erythroid cell specificity of B19 parvovirus.

ACKNOWLEDGMENTS

We thank Susan Cotmore and Peter Tattersall for the generous gift of pYT101 and pYT103 and Barrie Carter for very careful reading of the manuscript.

LITERATURE CITED

1. **Anderson, M. J., P. G. Higgins, L. R. Davis, J. S. Willman, S. E. Jones, I. M. Kidd, J. R. Pattison, and D. A. J. Tyrrell.** 1985. Experimental parvovirus infection in humans. J. Infect. Dis. **152**:257–265.
2. **Anderson, M. J., E. Lewis, I. M. Kidd, and B. J. Cohen.** 1984. An outbreak of erythema infectiosum associated with human parvovirus infection. J. Hyg. **93**:85–93.
3. **Becerra, S. P., J. A. Rose, M. Hardy, B. M. Baroudy, and C. W. Anderson.** 1985. Direct mapping of adeno-associated virus capsid proteins B and C: a possible ACG initiation codon. Proc. Natl. Acad. Sci. USA **82**:7919–7923.
4. **Berget, S. M., and B. L. Robberson.** 1986. U1, U2, and U4/U6 small nuclear ribonucleoproteins are required for in vitro splicing but not polyadenylation. Cell **46**:691–696.
5. **Berk, A. J., and P. A. Sharp.** 1977. Sizing and mapping of early adenovirus mRNAs by gel electrophoresis of S1 endonuclease-digested hybrids. Cell **12**:721–732.
6. **Birnstiel, M. L., M. Busslinger, and K. Strub.** 1985. Transcription termination and 3' processing: the end is in site! Cell **41**: 349–359.
7. **Brown, T., A. Anand, L. D. Ritchie, J. P. Clewley, and T. M. S. Reid.** 1984. Intrauterine human parvovirus infection and hydrops fetalis. Lancet **ii**:1033–1034.
8. **Carter, B. J.** 1984. Variant and defective interfering parvoviruses, p. 209–258. *In* K. I. Berns (ed.), The parvoviruses. Plenum Publishing Corp., New York.
9. **Carter, B. J., C. A. Laughlin, and C. J. Marcus-Sekura.** 1984. Parvovirus transcription, p. 153–208. *In* K. I. Berns (ed.), The parvoviruses. Plenum Publishing Corp., New York.
10. **Chen, K. C., B. C. Shull, E. A. Moses, M. Lederman, E. R. Stout, and R. C. Bates.** 1986. Complete nucleotide sequence and genome organization of bovine parvovirus. J. Virol. **60**:1085–1097.
11. **Chorba, T., P. Coccia, R. C. Holman, P. Tattersall, L. J. Anderson, J. Sudman, N. S. Young, E. Kurczynski, U. M. Sarrinen, R. Moir, D. N. Lawrence, J. M. Jason, and B. Evatt.** 1985. The role of parvovirus B19 in aplastic crisis and erythema infectiosum (fifth disease). J. Infect. Dis. **1514**:383–393.
12. **Cossart, Y. E., A. M. Field, B. Cant, and D. Widdows.** 1975. Parvovirus-like particles in human sera. Lancet **ii**:72–73.
13. **Cotmore, S. F., V. C. McKie, L. J. Anderson, C. R. Astell, and P. Tattersall.** 1986. Identification of the major structural and non-structural proteins encoded by human parvovirus B19 and mapping of their genes by procaryotic expression of isolated genomic fragments. J. Virol. **60**:548–557.
14. **Cotmore, S. F., and P. Tattersall.** 1984. Characterization and molecular cloning of a human parvovirus genome. Science **226**: 1161–1165.
15. **Favaloro, J., R. Treisman, and R. Kamen.** 1980. Transcription maps of polyomoa virus-specific RNA: analysis by two dimensional nuclease S1 gel mapping. Methods Enzymol. **65**:718–749.
16. **Gorman, C. M., L. F. Moffatt, and B. H. Howard.** 1982. Recombinant genomes which express chloramphenicol acetyltransferase in mammalian cells. Mol. Cell. Biol. **2**:1044–1051.
17. **Harper, M. E., L. M. Marselle, R. C. Gallo, and F. Wong-Staal.** 1986. Detection of lymphocytes expressing human T-lymphotropic virus type III in lymph nodes and peripheral blood from infected individuals by *in situ* hybridization. Proc. Natl. Acad. Sci. USA **83**:772–776.

18. **Jongeneel, C. V., R. Sahli, G. K. McMaster, and B. Hirt.** 1986. A precise map of splice junctions in the mRNAs of minute virus of mice, an autonomous parvovirus. J. Virol. **59**:564–573.
19. **Knott, P. D., G. A. C. Welply, and M. J. Anderson.** 1984. Serologically proven intrauterine infection with parvovirus. Br. Med. J. **289**:1660.
20. **Kozak, M.** 1984. Compilation and analysis of sequences upstream from the traditional start site in eukaryotic mRNAs. Nucleic Acids Res. **12**:857–872.
21. **Lebovitz, R. M., and R. G. Roeder.** 1986. Parvovirus H-1 expression: mapping of the abundant cytoplasmic transcripts and identification of promoter sites and overlapping transcription units. J. Virol. **58**:271–280.
22. **Maniatis, T., E. F. Fritsch, and J. Sambrook.** 1982. Molecular cloning: a laboratory manual. Cold Spring Harbor Laboratory, Cold Spring Harbor, N.Y.
23. **Melton, D. A., P. A. Krieg, M. R. Rebagliati, T. Maniatis, K. Zinn, and M. R. Green.** 1984. Efficient in vitro synthesis of biologically active RNA and RNA hybridization probes from plasmids containing a bacteriophage SP6 promoter. Nucleic Acids Res. **12**:7035–7056.
24. **Morgan, W. R., and D. C. Ward.** 1986. Three splicing patterns are used to excise the small intron common to all minute virus of mice RNAs. J. Virol. **60**:1170–1174.
25. **Mortimer, P. P., R. K. Humphries, J. G. Moore, R. H. Purcell, and N. S. Young.** 1983. A human parvovirus-like virus inhibits hematopoietic colony formation in vitro. Nature (London) **302**: 426–429.
26. **Ozawa, K., G. Kurtzman, and N. S. Young.** 1986. Replication of the B19 parvovirus in human bone marrow cell cultures. Science **233**:883–886.
27. **Ozawa, K., and N. Young.** 1987. Characterization of capsid and noncapsid proteins of B19 parvovirus propagated in human erythroid bone marrow cell cultures. J. Virol. **61**:2627–2630.
28. **Pattison, J. R., S. E. Jones, J. Hodgson, L. R. Davis, J. H. White, C. E. Stroud, and L. Murtaza.** 1981. Parvovirus infections and hypoplastic crisis in sickle cell anemia. Lancet **i**:664–665.
29. **Potter, H., L. Weir, and P. Leder.** 1984. Enhancer-dependent expression of human κ immunoglobulin genes introduced into mouse pre-B lymphocytes by electroporation. Proc. Natl. Acad. Sci. USA **81**:7161–7165.
30. **Reid, D. M., T. M. S. Reid, T. Brown, J. A. N. Rennine, and C. J. Eastmond.** 1985. Human parvovirus-associated arthropathy. Lancet **i**:419–421.
31. **Rhode, S. L.** 1985. *trans*-Activation of parvovirus P_{38} promoter by the 76K noncapsid protein. J. Virol. **55**:886–889.
32. **Schneider, R. J., B. Safer, S. M. Mumemitsu, C. E. Samuel, and T. Shenk.** 1985. Adenovirus VAI RNA prevents phosphorylation of the eukaryotic initiation factor 2 α subunit subsequent to infection. Proc. Natl. Acad. Sci. USA **82**:4321–4325.
33. **Shade, R. O., M. C. Blundell, S. F. Cotmore, P. Tattersall, and C. R. Astell.** 1986. Nucleotide sequence and genome organization of human parvovirus B19 isolated from the serum of a child during aplastic crisis. J. Virol. **58**:921–936.
34. **Sharp, P. A., A. J. Berk, and S. M. Berget.** 1980. Transcription maps of adenovirus. Methods Enzymol. **65**:750–768.
35. **Siegl, G., R. C. Bates, K. I. Berns, B. J. Carter, D. C. Kelly, E. Kurstak, and P. Tattersall.** 1985. Characteristics and taxonomy of *Parvoviridae*. Intervirology **23**:61–73.
36. **Srivastava, A., E. Lusby, and K. I. Berns.** 1983. Nucleotide sequence and organization of the adeno-associated virus 2 genome. J. Virol. **45**:555–564.
37. **Tratschin, J. D., J. Tal, and B. J. Carter.** 1986. Negative and positive regulation in *trans* of gene expression from adeno-associated virus vectors in mammalian cells by a viral rep gene product. Mol. Cell Biol. **6**:2884–2894.
38. **Treisman, R., N. J. Proudfoot, M. Shander, and T. Maniatis.** 1982. A single-base change at a splice site in a β^0-thalassemic gene causes abnormal RNA splicing. Cell **29**:903–911.
39. **Werner, D., Y. Chemla, and M. Herzberg.** 1984. Isolation of poly(A)$^+$ RNA by paper affinity chromatography. Anal. Biochem. **141**:329–336.
40. **White, D. G., A. D. Woolf, P. P. Mortimer, B. J. Cohen, D. R. Blake, and P. A. Bacon.** 1985. Human parvovirus arthropathy. Lancet **ii**:419–421.
41. **Wickens, M., and P. Stephenson.** 1984. Role of the conserved AAUAAA sequence: four AAUAAA point mutants prevent messenger RNA 3′ end formation. Science **226**:1045–1051.
42. **Young, N., M. Harrison, J. G. Moore, P. P. Mortimer, and R. K. Humphries.** 1984. Direct demonstration of the human parvovirus in erythroid progenitor cells infected in vitro. J. Clin. Invest. **74**:2024–2030.
43. **Young, N. S., P. P. Mortimer, J. G. Moore, and R. K. Humphries.** 1984. Characterization of a virus that causes transient aplastic crisis. J. Clin. Invest. **73**:224–230.
44. **Young, R. A., O. Hagenbuchle, and U. Schibler.** 1981. A single mouse α-amylase gene specifies two different tissue-specific mRNAs. Cell **23**:451–458.